RESEARCH ARTICLE

Performance of Some Basic Types of Road Barriers Subjected to the Collision of a Light Vehicle

R. R. Neves[a], H. Fransplass[b], M. Langseth[b], L. Driemeier[a], M. Alves[a]

[a] Group of Solid Mechanics and Structural Impact, University of Sao Paulo, Brazil;
[b] CASA, Centre for Advanced Structural Analysis, NTNU, Trondheim, Norway

ARTICLE HISTORY
Compiled October 4, 2017

ABSTRACT
The investigation of the performance of road barriers to the car collision is not very often studied in the the literature despite the importance of the topic to the passengers safety. Indeed, the various road barriers systems are seldom compared in terms of their capabilities in reducing the overall damage in an accident. Here, flexible and rigid road restraint system subjected to a 900 kg car impact are studied in detail via a finite element simulation, with the model being validated against experimental results. The model relies on dynamic material properties for the guardrail, which were measured in Split Hopkinson Pressure Bar. Three severity occupant indexes, ASI, THIV and PHD, are explored and used to infer road barriers behaviour when interacting with a light vehicle. It is also investigated the failure limit of bolted connections and its influence on the guardrail impact result by means of the car trajectory. According to test TB11 from EN 1317 standard, the impact simulation results using a 900kg car show that the flexible guardrail is safer than any of the analysed concrete barriers.

KEYWORDS
guardrail, crashworthiness, concrete barriers, severity occupant indexes

1. Introduction

Vehicle Restraint Systems (VRS), such as barriers, crash cushions and end terminals have an important role on the vehicle occupant safety. Particularly, the road barrier main function is to redirect an out of control vehicle back to the road, so avoiding collision or a dangerous veering off the road trajectory. Secondarily, the possible energy absorption offered by the barrier deformation or by any other energy dissipation method may be beneficial to the car occupant integrity [1].

As an example, it is estimated that only in Brazil there were in 2014, 52,226 deaths and 595,693 permanently disabled people related to traffic accidents [2, 3]. Despite of a possible poor car crashworthiness, driver negligence and other human failures, the lack of a good infra-structure contributes to the cause of this problem [4]. Hence, the proper design of road barriers, as discussed in [5], is a challenging task and optimization procedures have been used to improve the efficiency of these protective systems [**?**].

An important road barrier characteristic is the so called containment level. It is the capacity of the barrier to dissipate the vehicle's impact energy, which is different in

Corresponding author: M. Alves, maralves@usp.br

(a) Flexible (b) New Jersey (c) Vertical

Figure 1.: Barriers used in the present study. (a) metallic, (b) and (c) concrete.

metal guardrails when compared to concrete barriers. In general, the metal guardrail fits the *containment level*, ie it is able to withstand the impact of a 900 kg — 1500 kg vehicle. Concrete barriers have a *very high containment level*, handling the collision of a more than 30,000 kg vehicle. These levels are detailed in the European standard EN1317-2 [6]. A new generation of light and high containment level guardrails was studied experimentally in [7].

The pioneering work by [8] developed guardrail crash test performance guidelines for frontal and angled vehicle collisions. The report, known as NCHRP 350, was internationally accepted and inspired an update in the american AASHTO Manual for Assessing Safety Hardware (MASH). However, many countries do not present specific standard for evaluating safety performance of guardrails.

Reference [9] reports on instrumented crash tests against different barriers such as concrete, metal and temporary plastic water-filled. The authors also presented some real-world examples and emphasized the need for a closer relationship between road designers and car manufacturers with associated regulatory bodies in order to enhance car occupant safety. Another issue pointed out by the authors is the need of investigations on roadside barriers crashworthiness by instrumented crashes, as currently done with cars. This indicates that there is room for virtual analyses studies, given that they are less expensive.

Indeed, several authors [10–15] performed impact analyses using finite element FE techniques resulting in a satisfactory representation of a car crashing against a barrier. Reference [16] presented a literature review on road concrete barriers under impact loads, while [15] presented virtual impact analyses of metal defences operating under normal and irregular conditions.

In order to compare the behavior and the impact severity of a car occupant crashed against a road restraint system, the normalized test TB11 from EN 1317 standards [6, 17] was here studied. This test considers a car of 900 kg travelling at 100 km/h at a 20^o angle to the road restraint system. This scenario was represented by a finite element simulation to evaluate three different road restraint systems and their severity index to the car occupant. The analysed systems are highlighted in Figure 1 and comprise a metal guardrail, a New Jersey concrete barrier and a vertical concrete barrier.

The most common severity indexes used to estimate the consequences of a collision

on the vehicles occupants are the Acceleration Severity index (ASI), the Theoretical Head Impact Velocity (THIV) and the Post-impact Head Deceleration (PHD). In a crash test, the combination of these results gives a severity grade A, B or C according to Table 1. In this scale, grade A means low severity, with the THIV, ASI and PHD parameters lying below the human injury limits. Grades B and C implies higher severity injuries or even lethal consequences to the car occupants.

Table 1.: Severity index limits.

A	$ASI \leq 1.0$		
B	$1.0 < ASI \leq 1.4$	$THIV \leq 33km/h$	$PHD \leq 20g$
C	$1.4 < ASI \leq 1.9$		

The ASI is calculated by placing a virtual accelerometer in the modelled car center of gravity. It is computed during the whole event and its maximum value is used to evaluate the severity of the impact. If ASI exceeds 1.0 and 1.4 then it is considered that the impact event has dangerous or lethal consequences for the passengers, respectively.

For THIV, the occupant head is considered to be a freely moving object that, as the vehicle changes its speed during contact with the road barrier, continues moving until it strikes a surface within the interior of the vehicle. The PHD describes the head deceleration after this impact. Note that in the present study there is no modelling of the occupants as such. Rather, the analysis is based on acceleration levels numerically obtained in pre-defined positions of the car body and on the acceleration levels of a head like object hitting the inner surface of the car. This is seem as a good alternative to the modelling of the occupants given that it saves processing time and yet allows one to obtain the various indexes used for probing the overall barriers efficiency.

Metal W-beam guardrails are installed with different cross section posts, like C shape, wood, etc. Here a sigma, Σ, post was adopted, in accordance with the experimental data in [18]. Reference [19] investigated failure of W-beam bolt connections and suggested that a change in position at the connections significantly reduces the incidence of failure.

Preliminary simulations with 4 m spacing between posts indicated failure of the guardrail in redirecting the vehicle. This was not observed under the same conditions when the pole distance was 2 m. Therefore, all the simulations consider a space of 2 m between the posts. Also, the consideration of the soil and their property adds flexibility to the metal guardrail and makes the behavior of the system closer to real installation on highways. The soil finite element modelling was assessed experimentally and numerically in [20, 21]. Obviously, the mechanism of interaction between the post and the ground depends on the degree of soil compaction, which depends on the particular pole location. This adds to the high computational cost involved in the model so it was decided to leave aside the soil influence.

This study on road barriers performance in the scenario of car crash is here reported in 7 sections. In section 2, the vehicle finite element model and the methodology of occupant severity indices calculation are described. In section 3, the metal guardrail model description starts with the material characterization at low and high strain rates. The failure parameter for bolt connection between the w-beam and the sigma post failure is detailed as well as the performance calculation of the car in terms of the guardrail severity indices. It is here also offered a comparison with the experimental tests from literature. The vertical and New Jersey concrete barriers simulations and

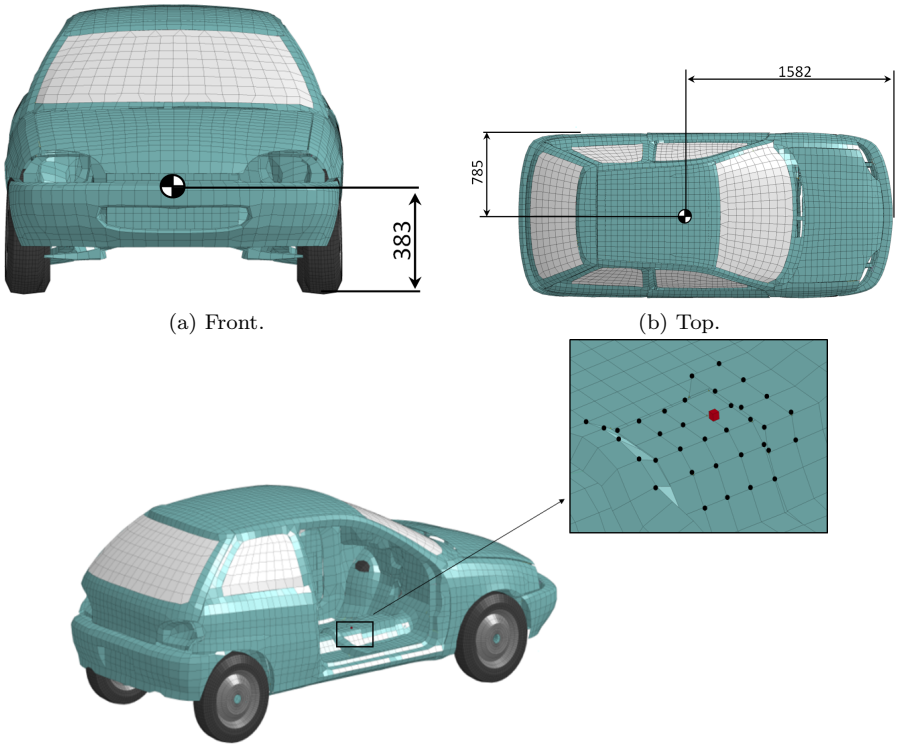

(a) Front.

(b) Top.

(c) Isometric.

Figure 2.: Car geometry with accelerometer position.

severity indices estimation are presented in section 4 and 5, respectively. The results are discussed in section 6, followed by the main conclusions from this study in section 7.

2. Car modelling

A deformable vehicle finite element model from the NCAC database [22] and adapted by Politecnico di Milano was used in the present study. The model, called Geo-Metro, is a light vehicle of 894 kg, Figure 2. This car model was chosen inasmuch it is quite close to the actual dimensions and weight of the cars used in the crash simulations reported in [17, 18, 23]. Besides, its full model is freely available so various numerical testes can be performed and compared to the experimental results of similar cars. The finite element model has 25037 finite elements and 28656 degrees of freedom. Shell elements were used to represent the structure of the vehicle; the power train, brake discs and callipers were modelled with solid elements; the rear suspension links were created using beam elements; springs and dampers were treated as discrete elements. In addition, various lumped masses were added at specific points to adequately characterize the overall vehicle inertia. An overview of the discretization is presented in Figure 2.

Due to the large deformation resulting from the impact event, the shell elements were set with 5 integration points throughout the thickness, ELFORM 16 (complete integration) in LS-Dyna. It was found during the impact simulations that in no part of the model the spurious modes exceeded 5% of the deformation energy. A linear elastic-

plastic material model was adopted and a simple failure criterion, set by a maximum plastic deformation of 50%, was used for all deformable elements of the car.

In order to calculate the severity index a virtual accelerometer was set to capture the acceleration history and angular displacement of the vehicle. This element is represented by a small rigid block near the center of gravity of the vehicle, as outlined in Figure 2c. In order to mitigate the existence of high frequency noise in its signal, the connection needs to be associated with a relevant mass component so 36 nodes from the vehicle structure were connected to the accelerometer. Considering these aspects, it was possible to obtain the acceleration history in all axes, $\bar{a}_x, \bar{a}_y, \bar{a}_z$, in the sensor position at the local coordinate system.

A good quality of the severity index post-processing was achieved by setting a data acquisition frequency of 100 kHz, relatively close to the magnitude order of the simulation time step $10^{-6}s$. A SAE 180Hz filter was applied before the severity index calculation. Hence, the vehicle dynamics was analyzed and undesirable effects of structural vibrations modes were eliminated. The ASI, $THIV$ and PHD indices were then calculated from the values of acceleration using the methodology below, which follows standard EN 1317-1 [17].

The ASI index is a scalar number calculated by

$$ASI(t) = \sqrt{\left(\frac{\bar{a}_x(t)}{\hat{a}_x}\right)^2 + \left(\frac{\bar{a}_y(t)}{\hat{a}_y}\right)^2 + \left(\frac{\bar{a}_z(t)}{\hat{a}_z}\right)^2}. \tag{1}$$

The variables $\hat{a}_x = 12g, \hat{a}_y = 9g, \hat{a}_z = 10g$ are the limits of acceleration for an occupant using seatbelts. The acceleration components $\bar{a}_x, \bar{a}_y$ and $\bar{a}_z$ were computed during the impact event of 50 ms. $g = 9.81$ m/s^2 is the gravitational acceleration.

To calculate THIV, it is assumed that at the beginning of the impact the head and the vehicle have a purely translational motion at the same horizontal speed. During the collision, it is considered that the vehicle moves only in the horizontal plane, therefore movements of roll, pitch or vertical translation are neglected, so that rollover is not considered here. THIV is obtained from,

$$THIV = \sqrt{\dot{x}_b^2\left(T_v\right) + \dot{y}_b^2\left(T_v\right)} \tag{2}$$

where $\dot{x}_b$ and $\dot{y}_b$ are the acceleration of the theoretical head in the x and y direction. The flight time T_v is defined by the instant the theoretical head position reaches any inner surface inside the vehicle in the horizontal plane. In the present case, the flight time was defined when the boundary conditions for the theoretical head displacement reaches a longitudinal displacement of 0.6 m or a lateral displacement of 0.3 m. $THIV$ is then defined when the first of these boundary conditions is achieved.

The abrupt deceleration of the head due to the impact on any inner surface of the vehicle can cause irreversible damage to the occupant when the acceleration is 20 times the gravitational acceleration. Therefore, the deceleration of the head after impact, described by the PHD index, is obtained by the maximum value of the acceleration resulting in the vehicle CG in the interval of 10 ms after the instant T_v, as follows,

$$PHD = \sqrt{\langle \ddot{x}_c \rangle^2 + \langle \ddot{y}_b \rangle^2}, \qquad for \qquad t \geq T_v. \tag{3}$$

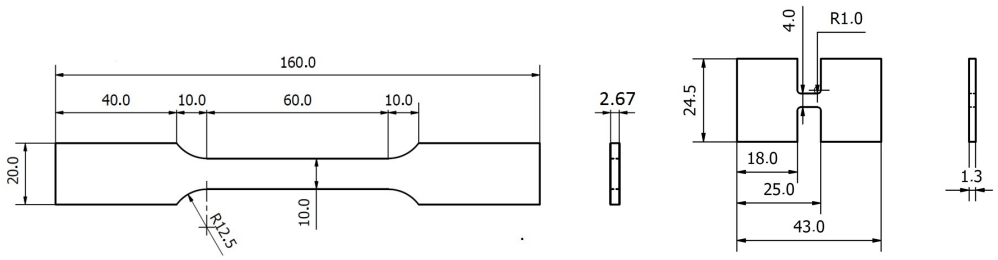

(a) Quasi-static. (b) High strain rate (SPHB).

Figure 3.: Specimens geometry for different strain rates.

3. Guardrail virtual model

3.1. *Material properties*

The W-beam material properties at low and high strain rates were measured so to have accurate material properties for the numerical simulations. The specimens were manufactured by laser cutting, according to the dimensions shown in Figure 3. High strain rate tests were performed in a Split Hopkinson Pressure Bar (SHPB). The geometry for the specimen in Figure 3b ensures uniform tension distribution concentrated mostly in the specimen neck, with a minimum portion of the deformed area distributed beyond this area, following studies from [24].

Figure 4 shows the quasi-static stress–strain curves in regions A, B and C of the W-beam. It is clear that regions A and C undergoes some sort of hardening due to the forming process. The yield strength in region B is slightly smaller than regions A and C. These differences were nevertheless disregarded in the simulations so allowing a simpler material model characterization. The W-beam cross-section was therefore considered homogeneous and it was assumed the material properties as the ones from region B.

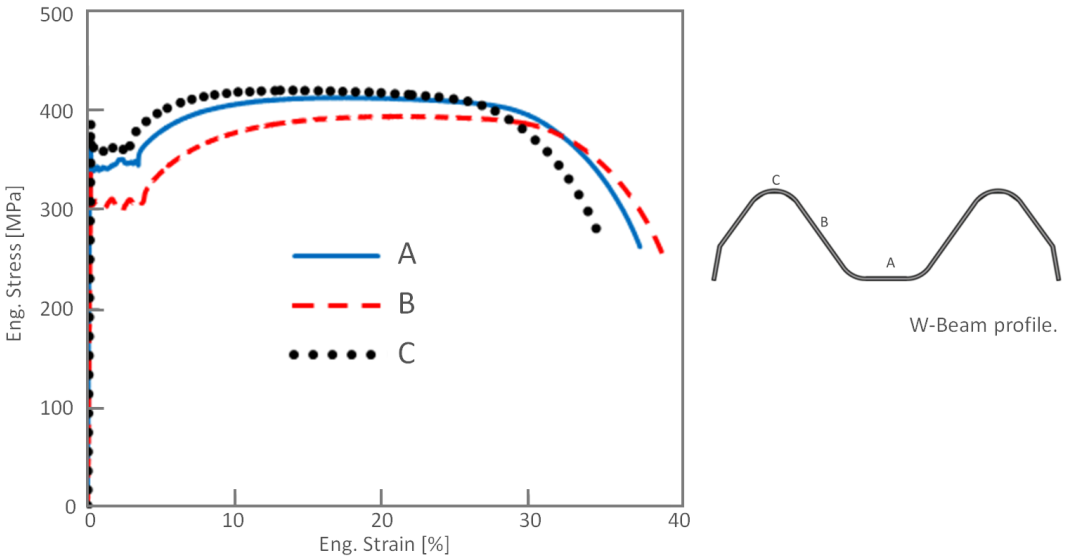

Figure 4.: Quasi-static stress-strain curves for W-beam material.

The specimens for high strain rates test were milled for thickness reduction and then

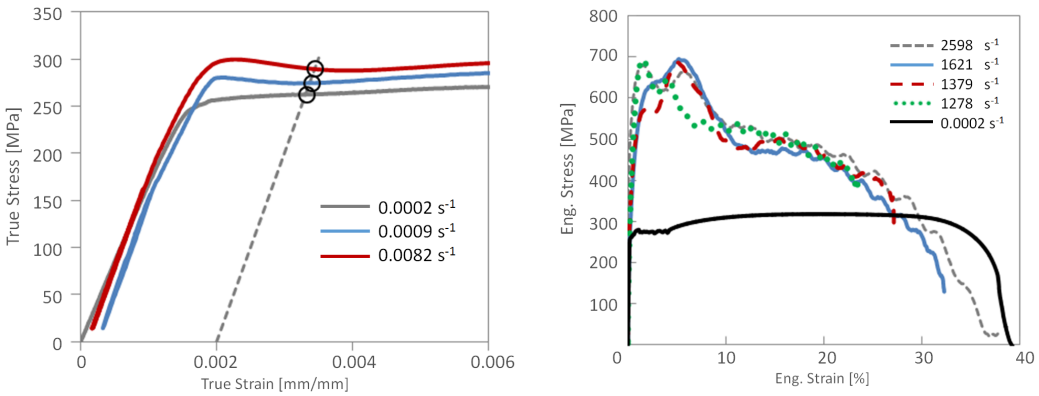

(a) Low strain rates.

(b) High strain rates.

Figure 5.: Stress strain curves at different strain rates.

grinded. Stress and strain curves at various high strain rates are plotted in Figure 5. For the low strain rate tests, the values of yield strength were obtained at 0.2% of total strain. For the dynamic tests, the true flow strength was defined at 20% of plastic deformation for the various strain rates. These data were later used for the calculation of the Cowper–Symonds material parameters [25].

The material model for the W-beam and post were defined according to the Cowper-Symonds constitutive model and read $C = 1016s^{-1}$ and $p = 5.7$, allowing the calculation of the dynamic flow stress as

$$\frac{\sigma}{\sigma_0} = 1 + \left(\frac{\dot{\epsilon}_p}{C}\right)^{1/p}, \tag{4}$$

where σ_0 is the static yield strength, σ the dynamic yield strength at strain rate $\dot{\epsilon}^p$. Other relevant material properties of the components are presented in Table 2. See [15] for Johnson-Cook parameters of the same material.

These material data for a typical guardrail are seem to be useful, let alone fundamental for the numerical modelling, inasmuch it gives information on the dynamic behaviour of the material after experiencing a manufacturing process.

Table 2.: Static mechanical properties adopted in metal guardrail simulations.

Component	Density kg/m^3	Elastic Modulus GPa	Poisson	Yield Stress MPa
W-beam	7850	200	0.3	256
Sigma post	7850	200	0.3	256

3.2. *Finite Element model*

The experimental tests conducted by [18] were reproduced virtually here using LS-Dyna. The experimental setup comprises a guardrail 84 m long, 0.75 m high (distance

between the ground plane and the post top), with posts lying 2 m apart along the barrier. The model includes the W-beam, sigma posts and anchorages, Figure 6. According to [18], the posts were fixed directly on the asphalt so that the post boundary condition was assumed clamped in the base, leading to an increase of the severity indexes.

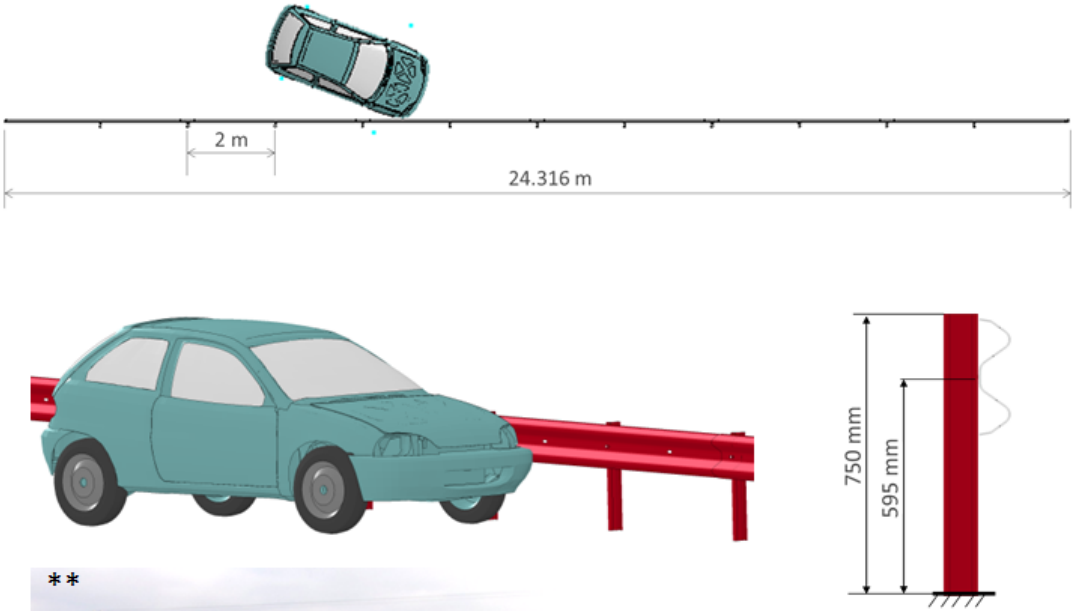

Figure 6.: Vehicle initial condition before impact (extracted from [18]).

A Peugeot 106, year 1991, of 903kg, impacted the barrier at a speed of 101.3 km/h, angle of 20^o in relation to the median plane of the guardrail. Figure 6 shows a picture of the initial condition of the impact test and the equivalent scenario simulation in finite element, where a 24.3 m long guardrail was used. This somewhat short guard-rail saves processing time.

The W-beam and post were modelled by finite elements as depicted in Figure 7. Six W-beams 4.3 m long were fixed in eleven posts displaced at 2 m. A total of 323,301 shell elements were used in the numerical model of the guardrail. The ends of the guardrail were clamped and the vehicle model was positioned between posts 4 and 5 at 20^o angle in relation to the guardrail. An initial speed of 27.78 m/s (100km/h) was applied in the longitudinal direction of the vehicle and an angular speed of 88.97 rad/s was set to the wheels. The W-beam was modelled mostly with 10 mm $\times$ 10 mm elements. The posts were discretized with 8 mm $\times$ 3 mm with further refinement of 3 mm $\times$ 3 mm on its base plus on W-beam contact area and 1.5 mm $\times$ 1.5 mm around the post hole. W-beam and posts were modelled with Belytschko-Tsay shell

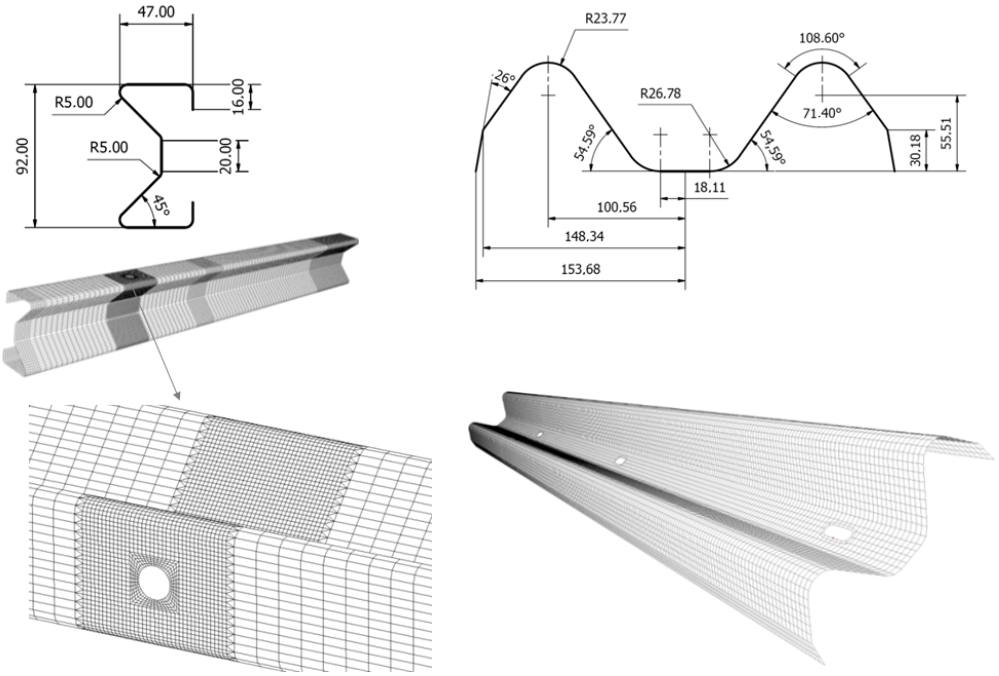

(a) Sigma post. (b) W-beam.

Figure 7.: Finite element mesh for post and beam. Connection area is detailed.

elements with four points of integration and reduced integration. Hourglass control type Flanagan-Belytschko was considered to avoid spurious modes.

In the experimental setup, the attachment of the W-beam with the posts is done by bolts. Also the superposition of the profiles W is fastened by eight bolts. In the virtual model, each bolt was replaced by a rigid massless beam whose behaviour on failure is defined by the average plastic strain of the fastened shell elements. Thereby, failure mechanism has an approximate ductile behaviour. The definition of these beams is analogous to the concept of a weld spot card represented in Figure 8. The overlapped profiles of W-beams have geometry offset of 3.1 mm to avoid node penetration in concordance regions, as illustrated in Figure 8b.

The contact between the surfaces of the vehicle and guardrail was defined with the coefficient of friction set to 0. The coefficient of friction between the wheel and the tire was set between 0.3 and 0.6.

3.3. *Bolt failure*

Material failure is a complex issue and many experimental [26], theoretical and numerical [27] studies have been performed in the development of failure criteria. In the present context, it has been disclosed that the bolts failure holding the guardrails to the post are of great importance. This is despite the study in [19] and the experimental results in [18], which show that failure in the guardrail occurs typically in the rail holes and not in the bolts.

Earlier failure of the bolts leads to such a detachment of the guardrail from the post that a colliding car can submerge under the guardrail, which would then fail to prevent the car from returning to the road. Likewise, a later failure of the bolt increases the occupants deceleration given that the whole structure becomes stiffer.

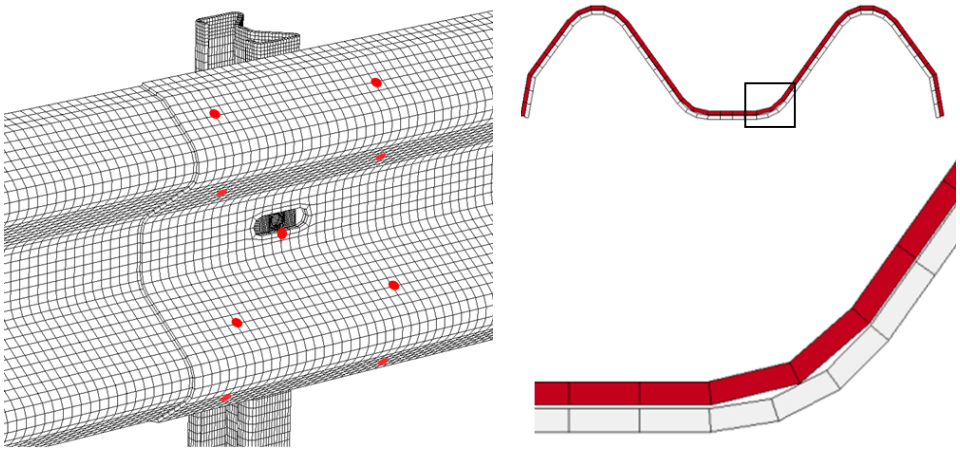

(a) Spot weld connections. (b) W-beam offset on overlay.

Figure 8.: Post and W-beam connection.

Failure of a bolt takes place at a microscale but an option to deal with the phenomenon at a macroscale is to define a global failure strain, PS, beyond which the bolt does not offer any further resistance to the separation of the guardrail from the post.

Parametric analyses for plastic strain failure values of $0.1 \leq PS \leq 0.9$ were performed in an attempt to evaluate the sensitivity of the defence response to the bolt strength. Based on the simulations results given on the graph and the images in Figure 9, it was possible to infer that the simulation and the experimental results are in good agreement when a good failure prediction of the connections is achieved.

Hence, for a plastic strain failure of $PS = 0.9$ it is noticed that the system redirects well the vehicle, leading to a good agreement between the numerical and experimental post-impact trajectories.

3.4. *Severity index results*

ASI, THIV and PHD curves versus time are shown in Figure 10. The figure also shows a comparison between the numerical simulation and the experimental tests of reference [18]. The simulation was performed with the bolt connection failure parameter set to $PS = 0.9$, with no friction between the contact surfaces, vehicle and guardrail. The labelled points in each curve indicate the severity indices in numerical and experimental cases.

From 0 to 0.1 s, the numerical ASI curve indicates a more severe acceleration experienced by the occupant than the respective experimental data, although the overall trend of both curves is rather similar. The numerical and experimental PHD and THIV indices are in quite good agreement.

Figure 11 shows a qualitative comparison between numerical and experimental test images at various instants. These results indicate a good representation of the impact event by the finite element model here developed, lending confidence to the virtual analysis.

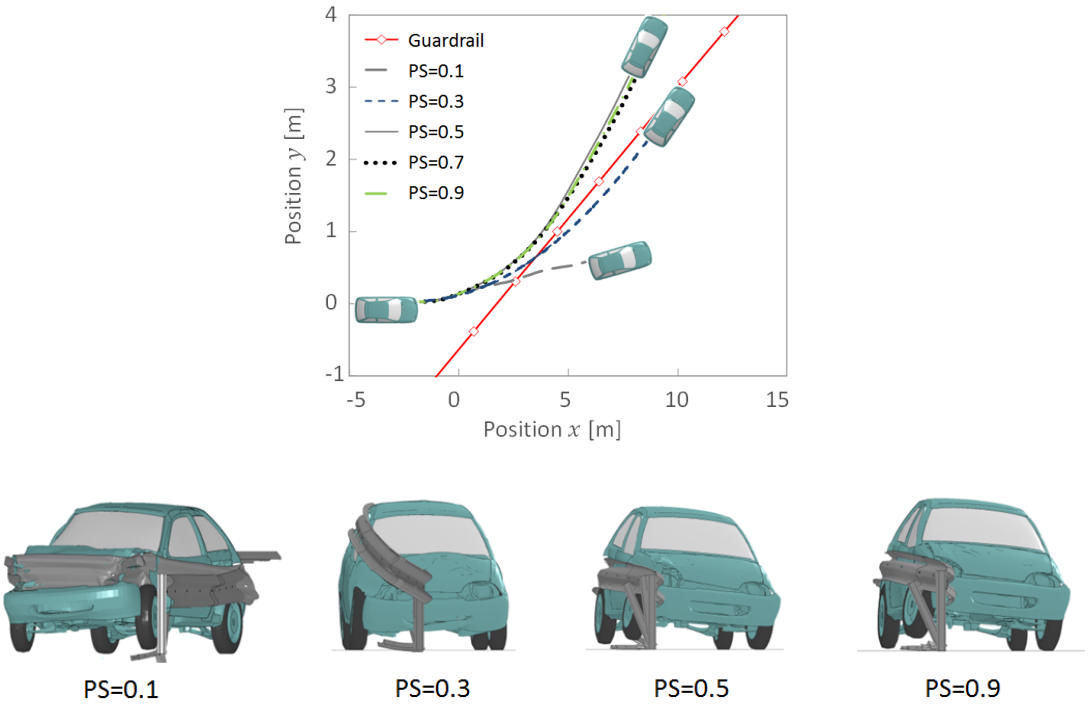

Figure 9.: Impact simulation for different plastic strain limits. Pictures extracted at time instant of 0.273s.

4. Vertical concrete barrier

The experimental test presented in [23] comprises a 900 kg Peugeot 205 Junior vehicle impacting a concrete barrier at 20^0 with a speed of 100.4 km/h. The barrier is made of 10 precast concrete blocks assembled with M20 bolts fixed at an angle of 45^0 with respect to the barrier vertical plane. Each precast concrete block is 3.15 m long and weighs 2,400 kg. Moreover, behind the barrier and exactly in the impact position, 3 concrete blocks were added, approximately 1,600 kg each, in order to avoid any displacement of the barrier. The concrete barrier ends were not anchored.

In view of the real test boundary conditions described above, the concrete barrier numerical model was ideally fixed to the ground. A total of 848 rigid solid elements composed the 25 m long rigid concrete barrier. In areas not affected by the impact event, element dimensions were set to 500 mm $\times$ 200 mm $\times$ 225 mm; the impact zone, with total lenght of 12 m, was discretized with elements 150 mm $\times$ 200 mm $\times$ 225 mm.

The static and dynamic friction coefficient for the contact between the vehicle and the barrier were varied in order to investigate the sensitivity of the impact event to this parameter and how it affects the severity indices. ASI, THIV and PHD curves from numerical and experimental results are depicted in Figure 13. It is clear that the simulation and experimental curves are in good agreement for a friction coefficient between $\mu = 0.05 - 0.1$.

The agreement for the ASI index occurs for $\mu = 0.2 - 0.3$. For THIV and PHD index, the simulation coefficient of friction set in $\mu = 0.05 - 0.10$ has the smallest deviation, -4.3% and 4.0% respectively. Note that, in general, the simulation with $\mu = 0.05 - 0.1$

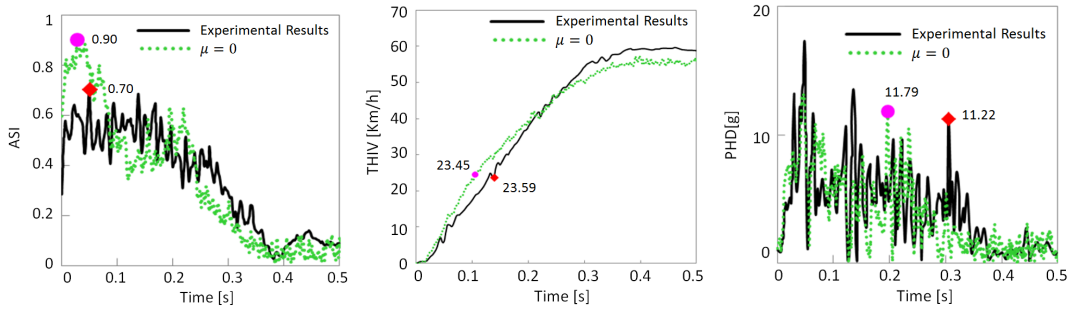

(a) ASI (b) THIV (c) PHD

Figure 10.: Severity index history during the car impact with the steel guardrail system.

retained an average deviation in all severity index of approximately 4.3% against 6.3% of the simulation $\mu = 0.2 - 0.3$ and 14.3% of $\mu = 0$ simulation.

The numerical analyses of the influence of the friction coefficient in the severity indices indicate that higher friction coefficients have a positive effect in the ASI and THIV indices, but the PHD index becomes worst.

Figure 14 compares the pictures of the experimental test performed in [17] with the simulation results.

5. New Jersey barrier

The next safety barrier is modelled according to the New Jersey profile, as shown in Figure 15. This type of barrier is commonly used in highway roads provisionally, during road construction, or permanently, to separate opposite lanes. When used as a road divider, it is fixed to the ground by means of a steel structure.

The New Jersey barrier is 25 m long, modelled with 884 solid elements. In the impact region, the elements are, on average, 149 mm $\times$ 69 mm, while in areas not affected by the impact the elements are around 500 mm $\times$ 69 mm. CONTACT AUTOMATIC SURFACE was used to establish the contact settings between the vehicle and the barrier. Friction coefficients, static and dynamic, were varied to investigate the sensitivity in the vehicle behaviour and occupant severity index.

Three impact scenarios were analysed with friction coefficients of $\mu = 0.05 - 0.1$, $\mu = 0.2$ and $\mu = 0.2 - 0.3$. In Figure 16 the simulation with the friction coefficient $\mu = 0.05 - 0.1$ is shown. Note that in the numerical model, the vehicle climbs the barrier before being redirected to the runway. This movement results in a partial dissipation of the impact energy. However, the vehicle shows a rollover trend as it approaches the ground, suggesting that this barrier may offer a more dangerous scenario for the occupants.

The severity index ASI, THIV and PHD obtained for the three simulations are plotted in Figure 17. The shape of the curves does not differ significantly, especially for the ASI and THIV indexes. The PHD curves show slight different deceleration peaks. All results are arranged in Table 3, including average and coefficient of variation (CV), in percentage.

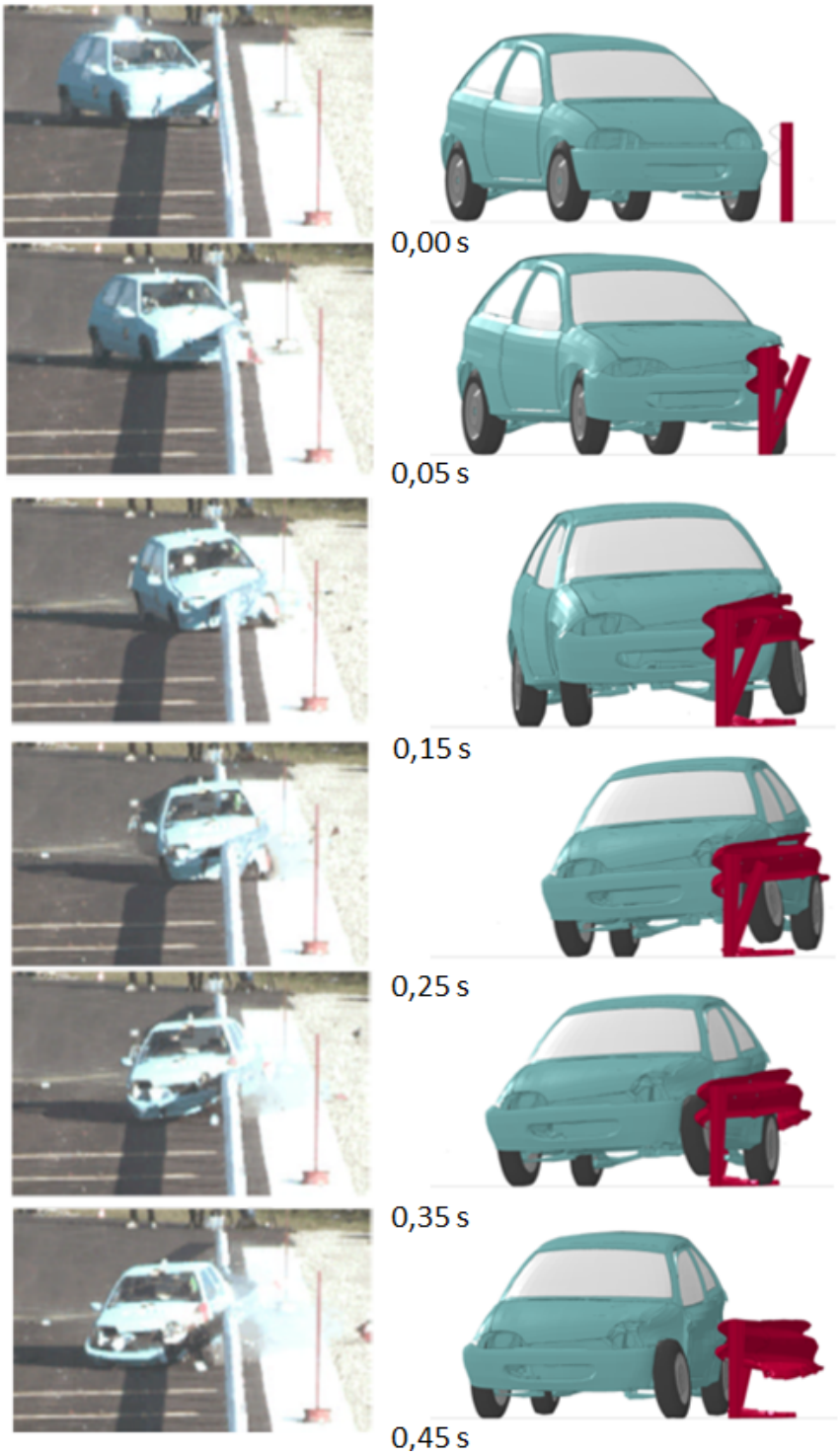

Figure 11.: Comparison between experimental tests, from [18] and numerical simulation.

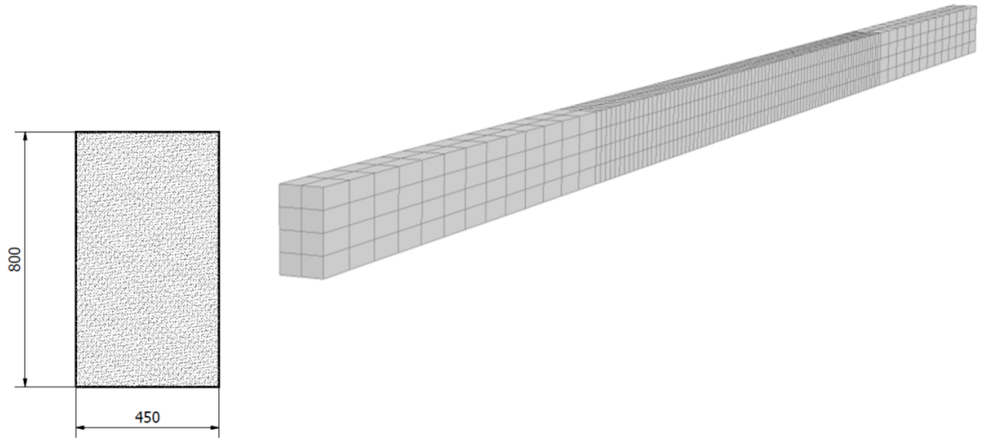

Figure 12.: Concrete barrier geometry and mesh.

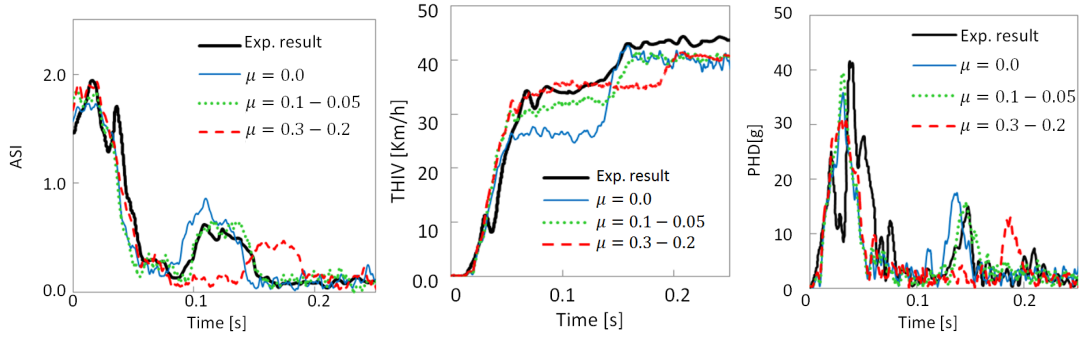

(a) ASI (b) THIV (c) PHD

Figure 13.: Severity index history within the car impact with vertical concrete barrier system.

6. Discussion

The present study addresses the virtual analysis of the impact of a light vehicle (900 kg) against three different types of road barriers: semi-rigid metal barrier, vertical and New Jersey rigid concrete barriers. The analyzes followed TB11 test specifications defined in [6]. The performance of the barriers was evaluated based on the ASI, THIV and PHD severity indexes. It should be noted that the design of this study did not take into consideration many important variables that play some role on the overall post crash scenario, like the road lateral angle. Some of these issues are discussed in [28]. Also, the study is limited to a single car model, ie the impact mass and structure were the same in the various simulations. Nevertheless, it is of importance that the numerical model correlated so well with the experimental results that firm conclusions can be taken regarding the overall barrier types performance. This is seem to be a contribution that can be benefit the ones acting in design of road barriers and cars.

The numerical results for the vertical concrete and metal barriers were validated with the results of real tests obtained from the literature [18, 23]. Comparison of numerical and experimental data showed a good correlation of the occupancy severity indexes. Comparison between images from the experimental tests extracted from the

Figure 14.: Comparison between test report [17] and numerical simulation.

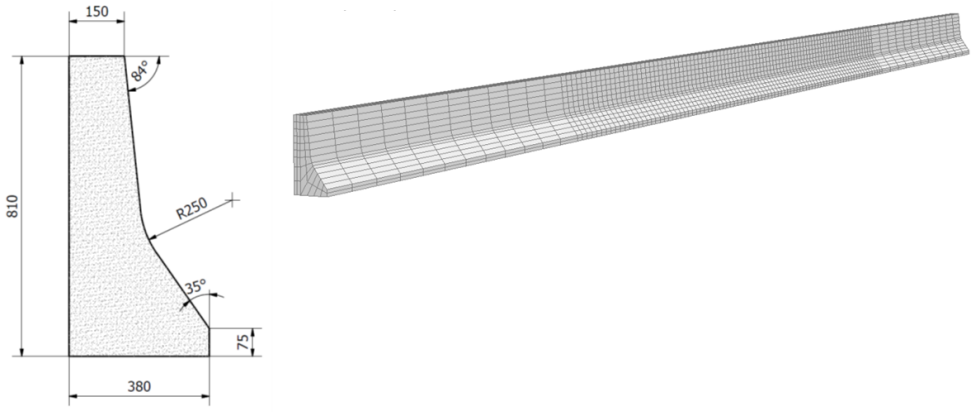

Figure 15.: New Jersey concrete barrier FEM and cross section details.

Table 3.: Severity indices for impact against a New Jersey concrete barrier.

Simulation	ASI $[-]$	THIV $[km/h]$	PHD $[g]$
$\mu = 0.1 - 0.5$	1.68	28.94	12.27
$\mu = 0.2 - 0.2$	1.70	31.81	9.43
$\mu = 0.3 - 0.1$	1.77	33.20	4.89
Average	1.72	31.32	8.86
CV (%)	2.8	6.9	42

literature and images of the simulations also gives an indication of the good quality of the model.

An appropriate definition of the failure parameter of the bolted connections in a metal barrier is crucial to the analysis, since there is a significant relationship between the correct redirection of the vehicle and that parameter. The results here obtained indicate that, for proper barrier modelling, a bolt failure strain of 0.9 gives good results.

The performance levels of the three road barriers analysed, measured by various severity indexes obtained by the finite element simulations, are summarized in Table 4. For the metal guardrail, $ASI = 0.7$ indicates that the acceleration of the occupant head did not exceed human limits. The THIV and PHD indexes are also below the limits of 33 km/h and 20g, respectively, so the metal barrier is scored with gravity level A, according to Table 1.

On the other hand, vertical and New Jersey concrete barriers exhibit higher ASI indices of 1.68 and 1.85, respectively. The ASI value above the acceptable range means that the impact can cause severe injuries to the vehicle's occupant. Although THIV and PHD indexes are below the limits, both concrete barriers are considered level C of occupant severity. In view of the ASI index, it can be stated that the rigid barriers offer twice the risk to the car occupants of a light vehicle when compared to the metal guardrail.

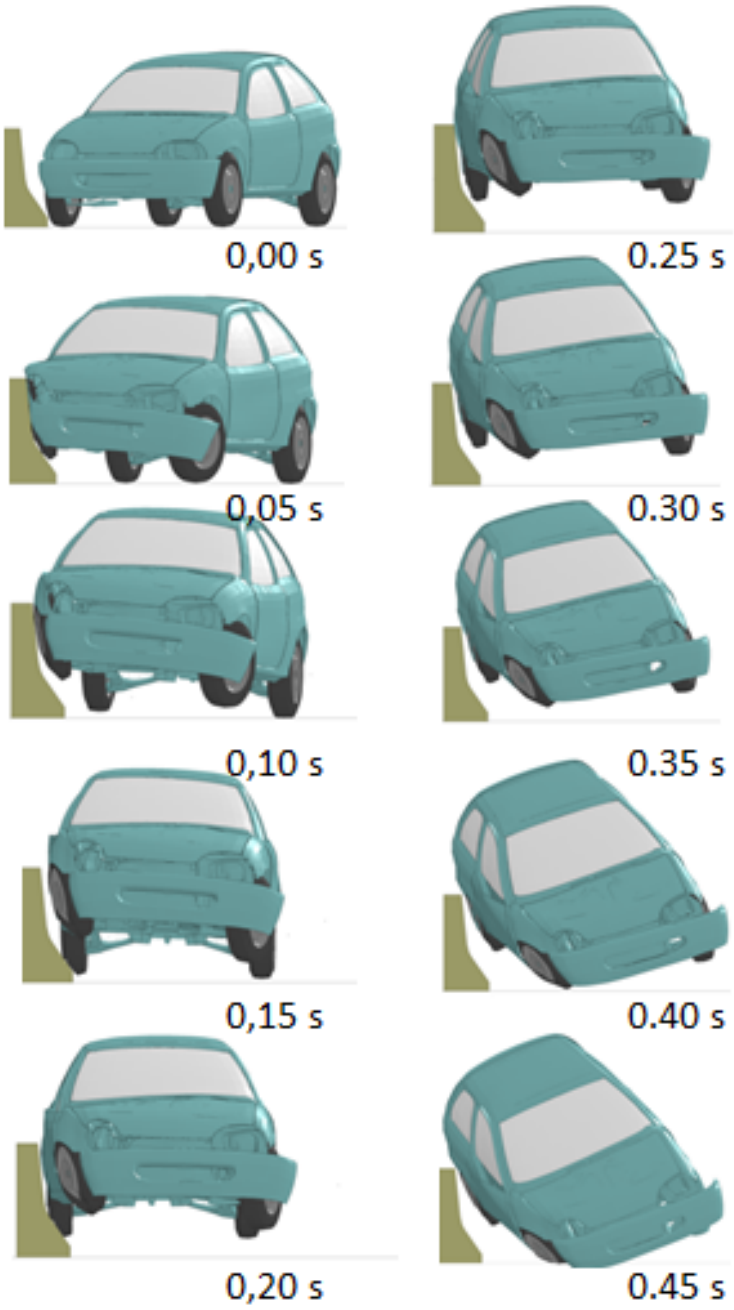

Figure 16.: Simulation of vehicle impact against New Jersey concrete barrier.

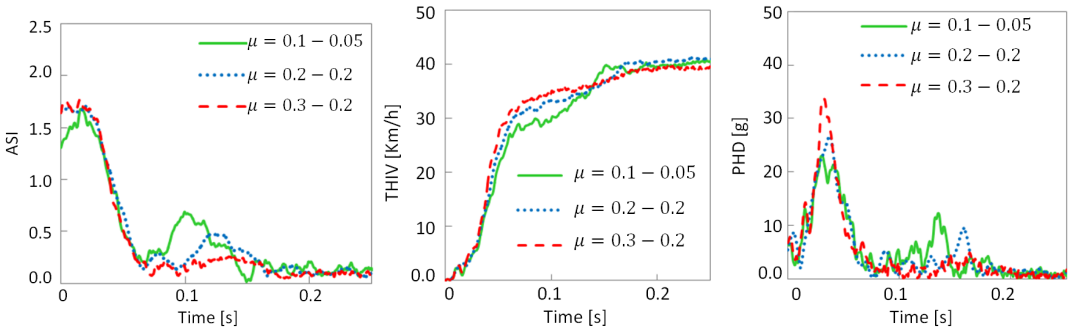

(a) ASI (b) THIV (c) PHD

Figure 17.: Severity index history within the car impact with New Jersey concrete barrier system.

Table 4.: Severity index comparison between the different types of road barrier systems.

Road Barrier	ASI $[-]$	THIV $[km/h]$	PHD $[g]$
metal guardrail	0.70	23.59	11.22
New Jersey concrete barrier	1.68	28.94	12.27
Vertical concrete barrier	1.85	30.61	15.60

7. Conclusions

In this paper, the performance of road barriers subject to the impact of a light vehicle was analysed according to the occupant severity indices ASI, THIV and PHD. The investigated road systems included: a metal guardrail with W-beam and sigma posts, vertical concrete barrier and a New Jersey concrete barrier. In this scenario, the study compares results of the impact phenomenon using finite element technique and experimental data from the literature. By demonstrating that the computational model reproduces well the real tests, it became possible to draw conclusions on the performance of various road barriers types.

The occupant severity indices calculated from various impact scenarios between car and different barriers indicate best impact scenarios for the occupants. Indeed, a light vehicle colliding against a metal guardrail is far better for the occupants than when colliding against concrete barriers. The ASI index greater than unity obtained for the concrete barriers indicates that human limits for theoretical acceleration of the occupant head were exceeded, which points to a lethal injury in such an impact scenario. This was not observed for the metal guardrail system.

On the other hand, one should be aware that metal guardrails may have a poor performance if jeopardised by poor assembling and installation procedures. It is also relevant to point out that further studies are necessary for accessing the overall crash scenario when a car hits a concrete barrier that is not fixed but rather just rests on a road. Friction issues here will lend to a complex scenario that deserves to be further explored in considering that such an assembly procedure is found when maintaining a

road.

References

[1] J. A. Hascall, R. K. Faller, J. D. Reid, and D. L. Sicking. Investigating the use of small-diameter softwood as guardrail posts (dynamic test results). Technical report, Madison, Wisconsin US: Forest Products Laboratory, 2007.

[2] M. Alves. Road fatalities among brazilian children: legislation and data analyses. In *Protection of Children in Cars: 13th International Conference, TÜV, München*, 2015.

[3] DPVAT. Boletim estatístico. Technical Report 4, Seguradora Líder - DPVAT, 2012.

[4] CNT. Pesquisa cnt de rodovias 2009: relatório gerencial. Technical report, Confederação Nacional de Transportes CNT, SEST, SENAT, 2009.

[5] T. Wenzel. The effect of recent trends in vehicle design on u.s. societal fatality risk per vehicle mile traveled, and their projected future relationship with vehicle mass. *Accid Anal Prev.*, 56:71–81, 2013.

[6] H. Yin, H. Fang, Q. Wang, and G. Wen. Design optimization of a MASH TL-3 concrete barrier using RBF-based metamodels and nonlinear finite element simulations. *Engineering Structures*, 114:122–134, 2016.

[7] EN1317-2 road restraint systems - part 2: Performance classes, impact test acceptance criteria and test methods for safety barriers.

[8] A. O. Atahan, A. Ö. Yüce, and M. M. Erdem. Crash testing and evaluation of a new generation l1 containment level guardrail. *Engineering Failure Analysis*, 38:25–37, 2014.

[9] H. E. Ross, D. L. Sicking, R. A. Zimmer, and J. D. Michie. Recommended procedures for the safety performance evaluation of highway features. Technical report, National Cooperative Highway Research Program, Report 350, National Academy Press, Washington, D.C., 1993.

[10] R. H. Grzebieta, R. Zou, T. Jiang, and A. Carey. Roadside hazard and barrier crashworthiness issues confronting vehicle and barrier manufactures and government regulators. Technical report, Monash University, Dept. of Civil Engineering, Australia, 2005.

[11] C. A. Plaxico, M. H. Ray, and K. Hiranmayee. Comparison of the impact performance of the G4(1W) and G4(2W) guardrail systems under NCHRP Report 350 Test 3-11 conditions. Technical report, Transportation Research Record 1720, TRB, Washington D.C., 2000.

[12] K. Sennah, M. Samaan, and A. Elmarakbi. Impact performance of flexible guardrail systems using ls-dyna. In *4th European LS-DYNA Users Conference*, 2003.

[13] X. Shen, L. Guo, L. Yang, X. Du, and P. Cao. Numerical analysis of impact effect on mechanical behavior of strong guardrail system. *Journal of Physics, Conference Series 96*, 2008.

[14] M. R. Ferdous, A. Abu-Odeh, R. P. Bligh adn H. L. Jones, and N. M. Sheikh. Performance limit analysis for common roadside and median barriers using ls-dyna. *International Journal of Crashworthiness*, 16(6):691–706, 2011.

[15] Giuseppina Amato, Fionn OBrien, Bidisha Ghosh, Gavin Williams, and Ciaran Simms. A scaling method for modelling the crashworthiness of novel roadside barrier designs. *International Journal of Crashworthiness*, 18(1):93–102, 2013.

[16] L. Driemeier, A. Yoneda, R. T. Moura, and M. Alves. Performance of metallic defences submitted to vehicle impact. *International Journal of Impact Engineering*, 21(3):252–277, 2016.

[17] M. F. B. M. Zain and H. J. Mohammed. Concrete road barriers subjected to impact loads: An overview. *Latin American Journal of Solids and Structures*, 12(10):1824–1858, 2015.

[18] EN1317-1 road restraint systems - part 1: Terminology and general criteria for test methods, 1998.

[19] LIER. Barrier test robust work package 4 - h2. Technical report, Laboratoire d'essais INRETS Equipements de la Route, 2004.

[20] M. H. Ray, C. A. Plaxico, and K. Engstrand. Performance of w-beam splices. In *80th Annual Meeting of the Transportation Research Board. Washington, D.C.: Worcester Polytechnic Institute*, 2001.

[21] A. Sassi and F. Ghrib. Development of finite element model for the analysis of a guardrail post subjected to dynamic lateral loading. *International Journal of Crashworthiness*, 19(5):457–468, 2014.

[22] W. Wu and R. Thomson. A study of the interaction between a guardrail post and soil during quasi-static and dynamic loading. *International Journal of Impact Engineering*, 34:883–898, 2007.

[23] NCAC. National crash analysis center. http://www.ncac.gwu.edu/. Accessed: 2014-05-30.

[24] LIER. Test report - round robin phase 2 tb11. Technical report, Laboratoire d'essais INRETS Equipements de la Route, 2002.

[25] J. V. Slycken. *Advanced use of a split hopkinson bar setup - application to TRIP steels.* PhD thesis, Academiejaar, 2008.

[26] M. Alves. Material constitutive law for large strains and strain rates. *Journal of Engineering Mechanics*, 126(2):215–218, 2000.

[27] Larissa Driemeier, Rafael T. Moura, Marcilio Alves, and Izabel Fernanda Machado. A bifailure specimen for accessing failure criteria performance. *International Journal of Plasticity*, 71:62–86, 2015.

[28] N. Tanlak, F.O. Sonmez, and E. Talay. Detailed and simplified models of bolted joints under impact loading. *Journal of Strain Analysis*, 46, 2010.

[29] M. Gutowski, E. Palta, and H. Fang. Crash analysis and evaluation of vehicular impacts on w-beam guardrails placed on sloped medians using finite element simulations. *Advances in Engineering Software*, in press, 2017.